LETTER • OPEN ACCESS

Attributing observed permafrost warming in the northern hemisphere to anthropogenic climate change

View the article online for updates and enhancements.

ENVIRONMENTAL RESEARCH
LETTERS

Attributing observed permafrost warming in the northern hemisphere to anthropogenic climate change

Lukas Gudmundsson[1,*] (ID), Josefine Kirchner[2] (ID), Anne Gädeke[3] (ID), Jeannette Noetzli[4,5] (ID) and Boris K Biskaborn[6] (ID)

1   Institute for Atmospheric and Climate Science, ETH Zürich, Zürich, Switzerland
2   Humboldt-Universität zu Berlin, Berlin, Germany
3   Potsdam Institute for Climate Impact Research, Member of the Leibniz Association, Telegrafenberg, 14412 Potsdam, Germany
4   WSL Institute for Snow and Avalanche Research SLF, Davos Dorf, Switzerland
5   Climate Change, Extremes and Natural Hazards in Alpine Regions Research Center CERC, Davos Dorf, Switzerland
6   Alfred Wegener Institute Helmholtz Centre for Polar and Marine Research, Potsdam, Germany
*   Author to whom any correspondence should be addressed.

E-mail: lukas.gudmundsson@env.ethz.ch

Abstract

Permafrost temperatures are increasing globally with the potential of adverse environmental and socio-economic impacts. Nonetheless, the attribution of observed permafrost warming to anthropogenic climate change has relied mostly on qualitative evidence. Here, we compare long permafrost temperature records from 15 boreholes in the northern hemisphere to simulated ground temperatures from Earth system models contributing to CMIP6 using a climate change detection and attribution approach. We show that neither pre-industrial climate variability nor natural drivers of climate change suffice to explain the observed warming in permafrost temperature averaged over all boreholes. However, simulations are consistent with observations if the effects of human emissions on the global climate system are considered. Moreover, our analysis reveals that the effect of anthropogenic climate change on permafrost temperature is detectable at some of the boreholes. Thus, the presented evidence supports the conclusion that anthropogenic climate change is the key driver of northern hemisphere permafrost warming.

1. Introduction

Permafrost, a subsurface feature of polar and alpine regions, is defined as ground that remains at or below 0 °C for many years. Permafrost influences the functioning of natural and human systems in high latitude and high altitude landscapes. State of the art Earth system models (ESM) unanimously project massive reductions in permafrost occurrence in response to man-made global warming (Burke *et al* 2020), which is particularly pronounced in polar and high mountain regions. This implies an increasing risk of permafrost warming and degradation with far-reaching consequences for both local environments and Earth system dynamics (IPCC 2019). For example, permafrost stores approximately twice as much carbon as the Earth's atmosphere currently holds (Schuur *et al* 2009). Through processes known

as the permafrost carbon feedback, a breakdown of organic carbon associated with permafrost degradation has the potential to release large amounts of greenhouse gases into the atmosphere and thus further contribute to global warming (Schuur *et al* 2015). Moreover, permafrost degradation can have significant effects on vegetation (Jin *et al* 2021) and tundra hydrology (Liljedahl *et al* 2016), damage infrastructure (Hjort *et al* 2018, Duvillard *et al* 2019), or impede winter overland transport (Gädeke *et al* 2021). In steep environments, permafrost warming has been associated with increasing magnitude and frequency of alpine mass movements such as rockfalls (Gruber and Haeberli 2007, Ravanel and Deline 2010, Marcer *et al* 2021).

Observational studies have documented systematic change of permafrost thermal state in recent years. For example, permafrost ground temperatures

have been shown to increase at regional (Etzelmüller *et al* 2020, Vasiliev *et al* 2020, Zhao *et al* 2020, Haberkorn *et al* 2021, Smith *et al* 2021) and global scales (Biskaborn *et al* 2019, Hock *et al* 2019, Noetzli *et al* 2020, Smith *et al* 2022). The main driver of permafrost warming is rising air temperature. But also additional heat introduced by precipitation (Mekonnen *et al* 2021) and effects related to changing snow insulation (Lawrence and Slater 2010) contribute. Permafrost warming is further modulated by ground properties, ground ice content, hydrology, or vegetation cover (Stuenzi *et al* 2021, Smith *et al* 2022).

Although permafrost warming is associated with rising air temperatures, the observed increase of permafrost temperature has to date not been unambiguously related to anthropogenic climate change. More precisely, it remains unclear whether increasing permafrost temperatures can be attributed to human-induced global warming or if natural climate variability is sufficient to explain the observed change. Such questions are addressed using climate change detection and attribution approaches, which are used for assessing impacts of anthropogenic emissions on the Earth's climate (Hegerl *et al* 2006, Bindoff *et al* 2013, Eyring *et al* 2021). Here the term detection refers to 'the process of demonstrating that an observed change is significantly different … from natural internal climate variability' (Hegerl *et al* 2006). Furthermore, attribution of an observed change to human emissions includes a 'demonstration that the detected change is consistent with simulated change driven by … anthropogenic changes in the composition of the atmosphere [e.g. greenhouse gas concentrations]…, and not consistent with alternative explanations of recent … change…' (Hegerl *et al* 2006). Traditionally, the focus of detection and attribution studies was put on large-scale climate indicators, including global temperatures (Jones *et al* 2013) or zonal precipitation (Zhang *et al* 2007). However, an increasing number of studies have attributed changes in terrestrial systems including in river flow (Gudmundsson *et al* 2017, 2021), water availability (Padrón *et al* 2020), drought indicators (Marvel *et al* 2019) and global lake systems (Grant *et al* 2021) to man-made climate change. Addressing the question of permafrost warming at the global scale, Guo *et al* (2020) demonstrated that the observed change in an air temperature-based permafrost index is not consistent with natural factors and that human emissions need to be considered as an explanatory cause.

While previous assessments show that the atmospheric drivers affecting permafrost are shifting in response to human emissions (Guo *et al* 2020), it is still not clear to which extent the effect of anthropogenic climate change is detectable in direct permafrost temperature observations. An unambiguous attribution of trends in permafrost temperatures is complicated by three factors.

First, permafrost monitoring is based on *in-situ* ground temperatures measured in boreholes (Noetzli *et al* 2021). Their installation and long-term operation at remote sites in cold climates are challenging. Therefore, they are limited in number, biased in their spatial distribution and hardly available for some regions (Hock *et al* 2019). Traditionally, data of these observatories were managed regionally or within research projects and institutions (Juliussen *et al* 2010, Permos 2021a), which further complicated global scale assessments. Only in the past decade, the Global Terrestrial Network for Permafrost (GTN-P) (Biskaborn *et al* 2015, Streletskiy *et al* 2021) has led efforts for collecting and curating long-term permafrost observations. Also, efforts like the World Meteorological Organization's Global Cryosphere Watch or the Terrestrial Multidisciplinary distributed Observatories for the Study of the Arctic Connections (Boike *et al* 2022) gained momentum for organization and sharing of long-term permafrost observations.

Second, natural climate and environmental variability often masks climate change signals at the station scale (Stott *et al* 2010). Therefore detection and attribution studies typically rely on heavy spatial or temporal aggregation over many locations for isolating climate change signals from internal climate variability (Bindoff *et al* 2013). This is, for example, done by averaging in space (e.g. global mean temperature (Jones *et al* 2013)) or by condensing temporal information to spatial trend patterns (e.g. regional river flow trends (Gudmundsson *et al* 2021)). The limited number of long-term permafrost observatories that are available in global collections may thus be a limiting factor. However, some features of permafrost temperature dynamics may facilitate a robust detection and attribution of climate change even at the station scale. In particular, the temporal variability of ground temperature is dampened with increasing depth, and observations at depth represent longer-term climatic changes (Biskaborn *et al* 2019). For example, with the amplitude of the seasonal cycle vanishes at the depth of the zero annual amplitude (DZAA), which is typically located around 15–20 m (Biskaborn *et al* 2019). Consequently, the response of ground temperature below DZAA to trends in atmospheric temperature is less affected by short-term variability, making it ideal for monitoring long-term climate change. Here we hypothesize that this natural filter contributes to reducing the effects of chaotic internal climate variability and hence enhances the visibility of potential climate signals.

Third, special properties of cold climate systems may further modify and even attenuate permafrost warming compared to rising air temperatures. For example, snow cover can have a considerable influence on ground temperatures as it insulates the ground from the atmospheric conditions. Moreover,

ice rich ground only little below 0 °C does not reflect increasing air temperatures by an increase in ground temperature as energy is consumed for the phase change (latent heat effects). In this phase, ground temperature remains more or less constant.

The objective of the paper is to test the hypothesis that human influence on the climate system is the key driver of observed permafrost warming. To this end, we employ the climate change detection and attribution approach and evaluate the likelihood of observed permafrost warming given estimates of pre-industrial climate variability and simulations of historical (HIST) climate change.

2. Data

2.1. Observed permafrost temperature

To ensure reproducibility we consider long observational permafrost temperature time series that stem from GTN-P (Biskaborn *et al* 2015, Streletskiy *et al*, 2021) and are available online (GTN-P 2021). They were selected based on their temporal coverage and quality prior to the International Polar Year (2007–2009) and aggregated to annual means and by Biskaborn *et al* (2019). The considered time series provide information at approximately DZAA. For this study, boreholes with at least 15 years of observations until 2014 were selected. We chose 2014 as a cut-off for the observations to match the end-date of the HIST ESM simulation experiments (see below). This results in the selection of 15 boreholes that cover the 37 year period 1978–2014 (figure 1). Note that not all boreholes have the same temporal coverage.

2.2. ESM simulations

We consider ground temperature time series stemming from ESM simulations. ESMs aim at capturing major aspects of Earth system dynamics by simulating ocean, atmosphere, and land systems in a coupled fashion. Land modules typically solve the water and energy balance and account also for cryosphere processes like snow dynamics. In ESMs, soils are represented through a stack of layers that can store and exchange energy and water and thus can simulate the thermal state of the sub-surface. For this study, ESM simulations contributing to the sixth phase of the Coupled Model Intercomparison Project (CMIP6) (Eyring *et al* 2016) are used. Long simulations driven with constant pre-industrial radiative forcing (PIC) are used to characterize internal climate variability without human influence (Eyring *et al* 2016). In a detection and attribution setup, these simulations can be used to assess how likely an observed change might have occurred due to internal climate variability alone. HIST simulations consider the effect of human emissions (greenhouse gases, aerosols) on the climate system throughout the past century until 2014 (Eyring *et al* 2016). In addition, HIST

simulations also account for natural variations in solar forcing and the effect of large volcanic eruptions. These simulations can be used to assess if an observed change is captured by ESMs driven with all relevant forcings. HIST natural (HIST-NAT) simulations are similar to HIST simulations but only account for variations in solar forcing and large volcanic eruptions throughout the past century (Gillett *et al* 2016). HIST-NAT simulations are used to investigate if naturally occurring variations in the radiative forcing are sufficient to capture observed trends using ESM simulations.

All CMIP6 data are prepared through a centralized pre-processing (Brunner *et al* 2020) that ensures consistency of the data and includes the interpolation of the model outputs to a common 2.5° grid. For HIST and HIST-NAT simulations, only data covering the time window of the observations are considered. The long PIC simulations are split into non-overlapping 37 year segments, each mimicking the observed period as if it could have occurred under pre-industrial conditions and with no variations in natural radiative forcing. Supplementary table S1 lists the considered models together with the number of available runs (HIST and HIST-NAT) or the number of available segments (PIC). In total, 659 (PIC), 500 (HIST), and 116 (HIST-NAT) samples are available for the considered experiments. Supplementary table S1 also lists the depth as well as the number of layers for each model.

2.3. Linking observations and ESM simulations

ESM simulations are compared to borehole data as follows. First only the grid-cells that contain boreholes are selected. Subsequently, years lacking observations are set to missing for each grid-cell individually. Due to differences in how ESMs represent shorelines in coarse grids, the number of available simulations can be reduced for boreholes in coastal regions. Supplementary table S2 lists the number of ESM simulations available at each borehole for all considered experiments. At each of these grid-cells, the soil-layer with the depth closest to the depth of observation is used. Since not all models cover the depth of observations, a sub-set of simulations with soil depths consistent with the depth of observations is also considered. See supplementary table S2 for the resulting number of simulations for each borehole and all experiments. Note also that no simulations from the HIST-NAT experiments are available for the borehole Janssonhaugen, Svalbard (Isaksen *et al* 2007) in the reduced ensemble.

Figure 2 shows the pre-processed time series of observed and simulated temperature anomalies at 17 m depth in rock glacier Murtèl-Corvatsch in the Swiss Alps, operated by the Swiss Permafrost Monitoring Network PERMOS (Permos 2021b). The time series are cantered to have a zero mean and years
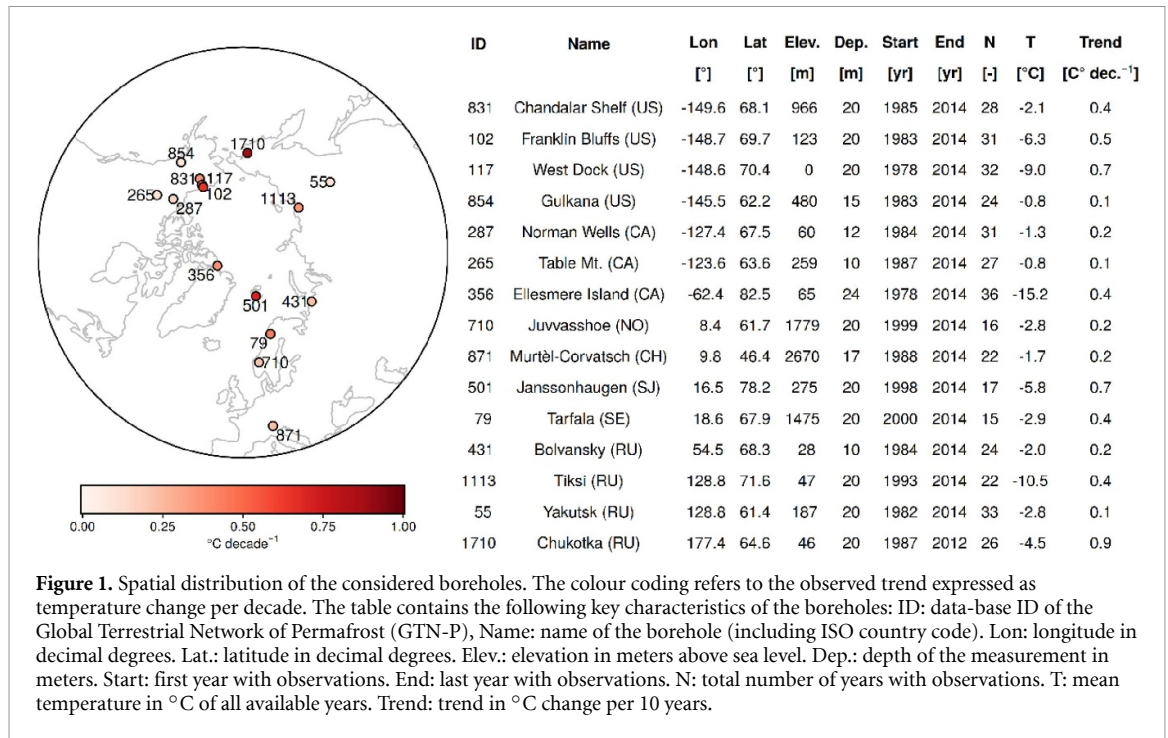
ID	Name	Lon [°]	Lat [°]	Elev. [m]	Dep. [m]	Start [yr]	End [yr]	N [-]	T [°C]	Trend [C° dec.⁻¹]
831	Chandalar Shelf (US)	-149.6	68.1	966	20	1985	2014	28	-2.1	0.4
102	Franklin Bluffs (US)	-148.7	69.7	123	20	1983	2014	31	-6.3	0.5
117	West Dock (US)	-148.6	70.4	0	20	1978	2014	32	-9.0	0.7
854	Gulkana (US)	-145.5	62.2	480	15	1983	2014	24	-0.8	0.1
287	Norman Wells (CA)	-127.4	67.5	60	12	1984	2014	31	-1.3	0.2
265	Table Mt. (CA)	-123.6	63.6	259	10	1987	2014	27	-0.8	0.1
356	Ellesmere Island (CA)	-62.4	82.5	65	24	1978	2014	36	-15.2	0.4
710	Juvvasshoe (NO)	8.4	61.7	1779	20	1999	2014	16	-2.8	0.2
871	Murtèl-Corvatsch (CH)	9.8	46.4	2670	17	1988	2014	22	-1.7	0.2
501	Janssonhaugen (SJ)	16.5	78.2	275	20	1998	2014	17	-5.8	0.7
79	Tarfala (SE)	18.6	67.9	1475	20	2000	2014	15	-2.9	0.4
431	Bolvansky (RU)	54.5	68.3	28	10	1984	2014	24	-2.0	0.2
1113	Tiksi (RU)	128.8	71.6	47	20	1993	2014	22	-10.5	0.4
55	Yakutsk (RU)	128.8	61.4	187	20	1982	2014	33	-2.8	0.1
1710	Chukotka (RU)	177.4	64.6	46	20	1987	2012	26	-4.5	0.9

Figure 1. Spatial distribution of the considered boreholes. The colour coding refers to the observed trend expressed as temperature change per decade. The table contains the following key characteristics of the boreholes: ID: data-base ID of the Global Terrestrial Network of Permafrost (GTN-P), Name: name of the borehole (including ISO country code). Lon: longitude in decimal degrees. Lat.: latitude in decimal degrees. Elev.: elevation in meters above sea level. Dep.: depth of the measurement in meters. Start: first year with observations. End: last year with observations. N: total number of years with observations. T: mean temperature in °C of all available years. Trend: trend in °C change per 10 years.
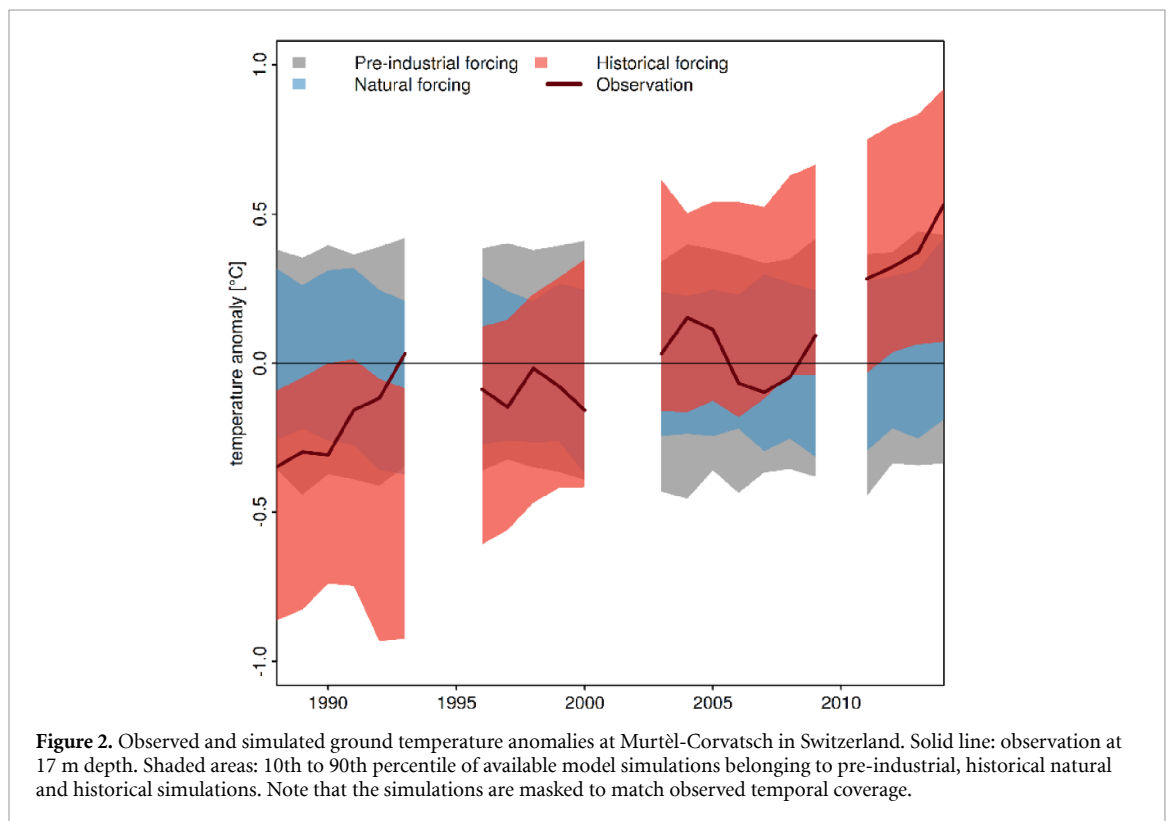

Figure 2. Observed and simulated ground temperature anomalies at Murtèl-Corvatsch in Switzerland. Solid line: observation at 17 m depth. Shaded areas: 10th to 90th percentile of available model simulations belonging to pre-industrial, historical natural and historical simulations. Note that the simulations are masked to match observed temporal coverage.

missing in the observed record are also set to zero in the simulations. Note also that the 10th to 90th percentile range of the model simulations is shown instead of individual runs to aid visualization. Data from all other boreholes are shown in supplementary figure S1 (all simulations) and figure S2 (simulations with depths that cover the depth of the observation).

3. Methods

3.1. Estimating trends

Change in observed and simulated ground temperature is quantified using linear trends in time estimated by ordinary linear regression at each location. Trends are expressed in units of °C change per decade

(i.e. 10 years). Subsequently the mean trend over all locations is computed. This procedure results in one northern hemisphere mean trend estimate for the observations and each simulation experiment.

3.2. Detection and attribution of anthropogenic climate change

Here we follow the abovementioned definition of climate change detection and attribution (Hegerl *et al* 2006) and evaluate the observed trend in the context of ESM simulation experiments with PIC, HIST and HIST-NAT radiative forcing. For each CMIP6 simulation experiment, we exploit the large number of samples available to construct the empirical trend distribution. Climate change detection can be claimed if the observed trend is unlikely given trends implied by the PIC simulations. To claim attribution to human induced climate change the following two conditions have to be fulfilled. First, the observed trend is consistent with (or likely given) the HIST simulations. Second, the observed trend is inconsistent with trends implied by HIST-NAT simulations. In other words, attribution can be claimed if the considered models only reproduce the observed trend if human influence on the climate system is considered.

The likelihood of the observed trend given the simulation experiments is quantified using approximate *p*-values defined as the fraction of simulated trends that are smaller than the observed trend. Very large or small values indicate that the observed trend is unlikely given the considered simulation experiment. In particular, large *p*-values suggest that the observed trend is larger than the expected trends. Here we follow the calibrated language of the intergovernmental panel on climate change (IPCC) (Chen *et al* 2021) and use $p > 0.66$ to indicate a likely, $p > 0.9$ to indicate a very likely and $p > 0.99$ to indicate virtually certain detection. Medium *p*-values (e.g. $p \approx 0.5$) indicate consistency between the observed and the simulated change.

4. Results

4.1. Comparing the spread of the full and the reduced model ensemble

We first compare the spread of the full ensemble with the reduced ensemble that only contains models that cover the depth of the observations (supplementary table S3). This shows that the variance of the full ensemble is unanimously larger than the variance of the reduced ensemble. This feature might be related to (a) the smaller sample size of the reduced ensemble or (b) to increased dampening of decadal variability in simulated ground temperature with increasing depth. Irrespective of the reasons for the difference in variance, the assessment of the full ensemble is therefore expected to be more conservative, i.e. it is less likely for observed trends to be located on the tails of the distributions implied by the simulations. To err on the

side of caution, the remainder of this paper therefore focuses on the full ensemble. However, all computations are repeated for the reduced ensemble and are presented in the supplement.
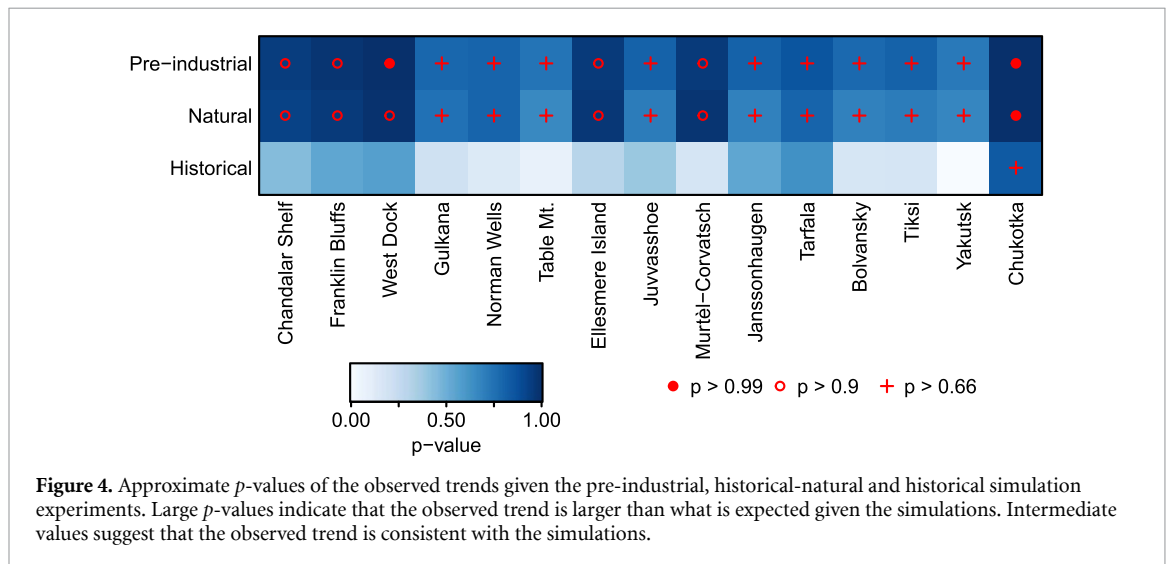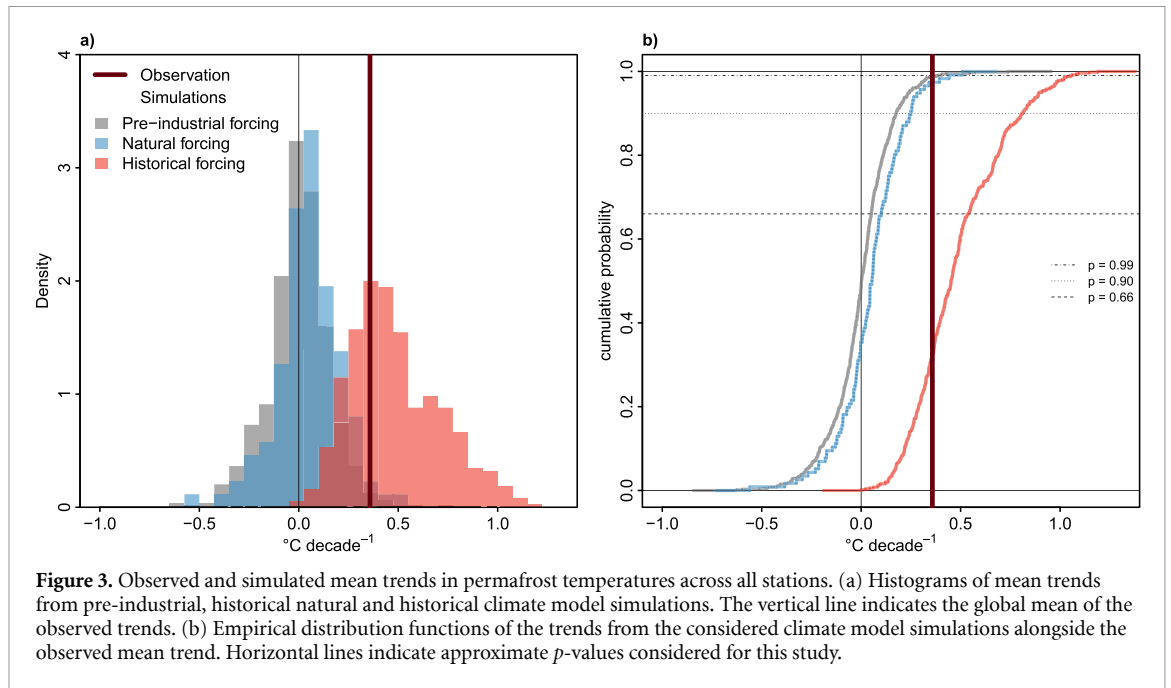
4.2. Mean trend over all boreholes

Observed and simulated mean trends across all boreholes are shown in figure 3(a). The mean trend in the observations increases at a rate of approximately 0.4 °C per decade. Mean trends found in PIC and HIST-NAT simulations fluctuate around zero. Moreover, the observed trend is with high certainty ($p > 0.99$) larger than trends that occur due to internal climate variability and very likely ($p > 0.9$) larger than trends related to naturally forced climate change (figure 3(b)). In contrast, trends of the HIST simulations clearly encompass the observed value. This shows that the observed mean trend can only be explained by ESM simulations that are driven with HIST radiative forcing that considers human emissions. In summary, the analysis presented in figure 3 shows that observed permafrost temperatures in the considered boreholes contain a detectable climate change signal (inconsistent with PIC) that can be attributed to anthropogenic climate change (consistency with HIST and inconsistency with HIST-NAT). A supplementary analysis that is based on the reduced ensemble confirms this result (supplementary figure S3).

4.3. Trends from individual boreholes

Given the significant results derived from the mean trend across all boreholes, we also investigate the likelihood of the observed trends at individual locations given the PIC, HIST-NAT, and HIST simulations. Figure 4 shows p-values of the observed trends at all locations for each simulation experiment. Despite the poor signal-to-noise ratio expected for the analysis of individual boreholes, *p*-values derived from the PIC and HIST-NAT simulations always exceed $p > 0.66$ and at six boreholes $p > 0.9$ or $p > 0.99$. This shows that observed trends in ground temperatures at all boreholes are at least likely larger than trends expected due to internal climate variability or naturally forced climate change alone. Moreover, at most boreholes, the observed trends are consistent with the HIST simulations that account for human influence on the climate system. Note that in some cases, very low *p*-values indicate that trends derived from HIST simulations can systematically exceed the observed trends. The latter result can be directly related to observed and simulated time series for which the simulated warming of HIST is smaller than the observed increase in temperature at the respective locations (supplementary figure S1).

Results based on the analysis of the reduced ensemble that only considers models that reach down to the depth of the observations is generally consistent

Figure 3. Observed and simulated mean trends in permafrost temperatures across all stations. (a) Histograms of mean trends from pre-industrial, historical natural and historical climate model simulations. The vertical line indicates the global mean of the observed trends. (b) Empirical distribution functions of the trends from the considered climate model simulations alongside the observed mean trend. Horizontal lines indicate approximate *p*-values considered for this study.

Figure 4. Approximate *p*-values of the observed trends given the pre-industrial, historical-natural and historical simulation experiments. Large *p*-values indicate that the observed trend is larger than what is expected given the simulations. Intermediate values suggest that the observed trend is consistent with the simulations.

with the results derived from the full ensemble (supplementary figure S4). Nonetheless, some differences are noted. For the PIC experiments, the approximate *p*-values of the reduced ensemble are generally larger ($p < 0.9$ in 10 of 15 cases), indicating a higher confidence in the detection of a systematic trend at the borehole scale. This, in turn, is consistent with the lower spread of the reduced ensemble (see supplementary table S3). Similar behaviour is found at most boreholes for the analysis of HIST-NAT. However, the latter result needs to be interpreted with caution since the reduced ensemble for HIST-NAT only has nine members at most locations, implying highly uncertain approximate *p*-values. Interestingly, the analysis of the HIST simulations of the reduced ensemble results in large approximate *p*-values ($p > 0.66$ and $p > 0.9$) at six locations. This implies that for these boreholes, the observed trends are significantly larger

than the trends of the HIST simulations in the constrained ensemble. In these cases, a careful inspection of the associated time series (supplementary figure S2) shows that the HIST simulations do exhibit a trend but underestimate the observed warming.

5. Discussion

The scope of this investigation is to assess the likelihood of observed trends in permafrost temperatures given simulations that account for natural and human influence on the climate system within the climate change detection and attribution framework (Hegerl *et al* 2006). To this end, permafrost temperature trends from selected long-term *in-situ* measurements are compared to empirical trend distributions derived from large ensembles of ESM simulations driven with

pre-industrial, HIST-NAT, and HIST radiative forcing. Thus, the analysis combined evidence from observations and ESMs using an empirical approach facilitated by many available samples for each of the considered simulation experiments.

We note that the empirical approach to climate change detection and attribution makes the analysis potentially sensitive to the finite sample of simulations used to estimate distributions. Furthermore, the choice to consider the ensemble of opportunity within the CMIP6 archive puts more weight on models with more initial condition ensemble members or longer pre-industrial control simulations. However, theoretically more sophisticated approaches for climate change detection and attribution make strong assumptions regarding the underlying statistical model, typically including the normality of residuals as well as additivity of forced response and internal climate variability (Allen and Stott 2003, Ribes *et al* 2016). While such assumptions are often meaningful and required for enhancing the signal-to-noise ratio, the resulting methods add complexity and uncertainty to the analysis. The presented study, in turn, takes full advantage of the abundance of ESM integrations to empirically approximate the distributions of permafrost trends given different radiative forcing.

We also note uncertainties related to simplified modelling assumptions, which are necessary when simulating thermal properties of soils in ESMs at the global scale. For example, there is a scale mismatch between boreholes and the resolution of the models. Moreover, models differ significantly in the maximum ground depth and the number of considered soil layers. In addition, imperfect model physics and un-resolved processes may cause model errors. Moreover, ESM temperatures can be biased leading to differences in absolute values compared to observations. Finally, not all considered ESMs reach down to the depth of the observations.

Besides model uncertainties, limits of the observational record must be considered for a balanced assessment of the evidence. Most importantly, only boreholes compiled by Biskaborn *et al* (2019) that are publicly available (GTN-P 2021) were used to ensure reproducibility. Furthermore, the availability of climate model simulations implied that only observations until 2014 were used, which further reduces the likelihood of discriminating systematic trends against internal climate variability. In addition, point-scale ground temperature observations are considerably influenced by natural environmental (e.g. ground characteristics and surface cover) and climate variability (e.g. small-scale variations in air temperature and precipitation), which can obscure underlying climate change signals.

To alleviate these issues the following measures for enhancing the signal to noise ratio were taken: first, focussing on permafrost temperatures at DZAA

was a guiding feature when designing the analysis. At DZAA, permafrost temperatures have negligible intra-annual and reduced year-to-year variability compared to surface temperatures. Therefore, they are less influenced by short-term climatic fluctuations. Second, the analysis focussed on comparing long-term trends, which are driven by overarching shifts in climatic conditions. Third, the primary analysis of this paper focused on the mean trend across all boreholes which reduced effects of natural spatial variability and hence further increased the signal to noise ratio. In addition, a supplementary analysis confirmed the validity of the results when only considering ESMs with soil depths that are consistent with the observations.

6. Conclusions

In conclusion the analysis supports a high degree of confidence in the finding that the observed mean trend in permafrost temperature across all boreholes is inconsistent with internal climate variability and that that ESM simulations only capture the observed mean trend if human influence on the climate system is considered. In addition, a secondary analysis finds an influence of anthropogenic global warming on permafrost temperature at the borehole scale. Despite the reduced statistical confidence this is remarkable, since detecting and attributing climate change at individual locations is generally considered to be hampered by large degrees of environmental and climate variability (Zwiers and Zhang 2003, Stott *et al* 2010).

Although the results provide considerable evidence in support of the hypothesis that human influence on the climate system is driving observed permafrost temperature warming, we note that the results only represent what is possible with the latest generation of ESMs and the considered observations. Therefore, the findings should not be interpreted in isolation. Here it is essential to recall that the presented research is fully consistent with current understanding of impacts of anthropogenic climate change on permafrost (IPCC 2019, Burke *et al* 2020, Guo *et al* 2020). Nonetheless, a strong need for continuous and global efforts to observe and share permafrost temperature remains to monitor climate change impacts and to foster climate adaptation in environments with amplified warming rates such as the Arctic and Mountain regions.

In summary, this study shows that the mean permafrost temperature trend across 15 boreholes around the northern hemisphere can only be explained by ESM simulations, if effects of human emissions on the climate system are considered and that systematic climate change patterns are emerging at the borehole scale. Consequently, the combined analysis of spatial mean trends across locations and the assessment of individual boreholes supports the

hypothesis that observed permafrost warming can be attributed to anthropogenic climate change.

ORCID iDs

Lukas Gudmundsson ⬥ https://orcid.org/0000-0003-3539-8621
Josefine Kirchner ⬥ https://orcid.org/0000-0003-0294-0998
Anne Gädeke ⬥ https://orcid.org/0000-0003-0514-2908
Jeannette Noetzli ⬥ https://orcid.org/0000-0001-9188-6318
Boris K Biskaborn ⬥ https://orcid.org/0000-0003-2378-0348

References

Allen M R and Stott P A 2003 Estimating signal amplitudes in optimal fingerprinting, part I: theory *Clim. Dyn.* **21** 477–91

Bindoff N L *et al* 2013 Detection and attribution of climate change: from global to regional *Climate Change 2013: The Physical Science Basis. Contribution of Working Group I to the Fifth Assessment Report of the Intergovernmental Panel on Climate Change* ed T F Stocker *et al* (Cambridge: Cambridge University Press)

Biskaborn B K *et al* 2019 Permafrost is warming at a global scale *Nat. Commun.* **10** 264

Biskaborn B K, Lanckman J-P, Lantuit H, Elger K, Streletskiy D A, Cable W L and Romanovsky V E 2015 The new database of the Global Terrestrial Network for Permafrost (GTN-P) *Earth Syst. Sci. Data* **7** 245–59

Boike J *et al* 2022 Standardized monitoring of permafrost thaw: a user-friendly, multiparameter protocol *Arct. Sci.* **8** 153–82

Brunner L, Hauser M, Lorenz R and Beyerle U 2020 *The ETH Zurich CMIP6 Next Generation Archive: Technical Documentation* (https://doi.org/10.5281/zenodo.3731088)

Burke E J, Zhang Y and Krinner G 2020 Evaluating permafrost physics in the Coupled Model Intercomparison Project 6 (CMIP6) models and their sensitivity to climate change *Cryosphere* **14** 3155–74

Chen D *et al* 2021 Framing, context, and methods *Climate Change 2021: The Physical Science Basis. Contribution of Working Group I to the Sixth Assessment Report of the Intergovernmental Panel on Climate Change* ed V Masson-Delmotte *et al* (Cambridge: Cambridge University Press)

Streletskiy D, Noetzli J, Smith S L, Vieira G, Schoeneich P, Hrbacek F *et al* 2021 Measurement standards and monitoring guidelines for the global terrestrial network for permafrost (GTN-P) 2021-2021 (https://gtnp.arcticportal.org/)

Duvillard P-A, Ravanel L, Marcer M and Schoeneich P 2019 Recent evolution of damage to infrastructure on permafrost in the French Alps *Reg. Environ. Change* **19** 1281–93

Etzelmüller B, Guglielmin M, Hauck C, Hilbich C, Hoelzle M, Isaksen K, Noetzli J, Oliva M and Ramos M 2020 Twenty years of European mountain permafrost dynamics—the PACE legacy *Environ. Res. Lett.* **15** 104070

Eyring V, Bony S, Meehl G A, Senior C A, Stevens B, Stouffer R J and Taylor K E 2016 Overview of the Coupled Model Intercomparison Project Phase 6 (CMIP6) experimental design and organization *Geosci. Model Dev.* **9** 1937–58

Eyring V *et al* 2021 Human influence on the climate system *Climate Change 2021: The Physical Science Basis. Contribution of Working Group I to the Sixth Assessment Report of the Intergovernmental Panel on Climate Change* ed V Masson-Delmotte *et al* (Cambridge: Cambridge University Press)

Gädeke A, Langer M, Boike J, Burke E J, Chang J F, Head M, Reyer C P O, Schaphoff S, Thiery W and Thonicke K 2021 Climate change reduces winter overland travel across the Pan-Arctic even under low-end global warming scenarios *Environ. Res. Lett.* **16** 024049

Gillett N P, Shiogama H, Funke B, Hegerl G, Knutti R, Matthes K, Santer B D, Stone D and Tebaldi C 2016 The detection and attribution model intercomparison project (DAMIP v1.0) contribution to CMIP6 *Geosci. Model Dev.* **9** 3685–97

Grant L *et al* 2021 Attribution of global lake systems change to anthropogenic forcing *Nat. Geosci.* **14** 849–54

Gruber S and Haeberli W 2007 Permafrost in steep bedrock slopes and its temperature-related destabilization following climate change *J. Geophys. Res.* **112** F02S18

GTN-P 2021 Long-term mean annual ground temperature data for permafrost (https://doi.org/10.1594/PANGAEA.930669)

Gudmundsson L *et al* 2021 Globally observed trends in mean and extreme river flow attributed to climate change *Science* **371** 1159–62

Gudmundsson L, Seneviratne S I and Zhang X 2017 Anthropogenic climate change detected in European renewable freshwater resources *Nat. Clim. Change* **7** 813–6

Guo D, Sun J, Li H, Zhang T and Romanovsky V E 2020 Attribution of historical near-surface permafrost degradation to anthropogenic greenhouse gas warming *Environ. Res. Lett.* **15** 084040

Haberkorn A, Kenner R, Noetzli J and Phillips M 2021 Changes in ground temperature and dynamics in mountain permafrost in the Swiss Alps *Front. Earth Sci.* **9** 626686

Hegerl G C, Karl T R, Allen M, Bindoff N L, Gillett N, Karoly D, Zhang X and Zwiers F 2006 Climate change detection and attribution: beyond mean temperature signals *J. Clim.* **19** 5058–77

Hjort J, Karjalainen O, Aalto J, Westermann S, Romanovsky V E, Nelson F E, Etzelmüller B and Luoto M 2018 Degrading permafrost puts Arctic infrastructure at risk by mid-century *Nat. Commun.* **9** 5147

Hock R *et al* 2019 High mountain areas *IPCC Special Report on the Ocean and Cryosphere in a Changing Climate* ed H-O Pörtner *et al* (Cambridge, UK : Cambridge University Press) pp 131–202 accepted

IPCC 2019 *IPCC Special Report on the Ocean and Cryosphere in a Changing Climate* (Cambridge, UK: Cambridge University Press) (https://doi.org/10.1017/9781009157964)

Isaksen K, Sollid J L, Holmlund P and Harris C 2007 Recent warming of mountain permafrost in Svalbard and Scandinavia *J. Geophys. Res.* **112** F02S04

Jin X-Y, Jin H-J, Iwahana G, Marchenko S S, Luo D-L, Li X-Y and Liang S-H 2021 Impacts of climate-induced permafrost degradation on vegetation: a review *Adv. Clim. Change Res.* **12** 29–47

Jones G S, Stott P A and Christidis N 2013 Attribution of observed historical near−surface temperature variations to anthropogenic and natural causes using CMIP5 simulations *J. Geophys. Res.* **118** 4001–24

Juliussen H, Christiansen H H, Strand G S, Iversen S, Midttømme K and Rønning J S 2010 NORPERM, the Norwegian permafrost database—a TSP NORWAY IPY legacy *Earth Syst. Sci. Data* **2** 235–46

Lawrence D M and Slater A G 2010 The contribution of snow condition trends to future ground climate *Clim. Dyn.* **34** 969–81

Liljedahl A K *et al* 2016 Pan-Arctic ice-wedge degradation in warming permafrost and its influence on tundra hydrology *Nat. Geosci.* **9** 312–8

Marcer M, Cicoira A, Cusicanqui D, Bodin X, Echelard T, Obregon R and Schoeneich P 2021 Rock glaciers throughout the French Alps accelerated and destabilised since 1990 as air temperatures increased *Commun. Earth Environ.* **2** 81

Marvel K, Cook B I, Bonfils C J W, Durack P J, Smerdon J E and Williams A P 2019 Twentieth-century hydroclimate changes consistent with human influence *Nature* **569** 59–65

Mekonnen Z A, Riley W J, Grant R F and Romanovsky V E 2021 Changes in precipitation and air temperature contribute comparably to permafrost degradation in a warmer climate *Environ. Res. Lett.* **16** 024008

Noetzli J *et al* 2021 Best practice for measuring permafrost temperature in boreholes based on the experience in the Swiss Alps *Front. Earth Sci.* **9** 607875

Noetzli J, Christiansen H H, Isaksen K, Smith S, Zhao L and Streletskiy D A 2020 Permafrost thermal state [in "State of the Climate in 2019"] *Bull. Am. Meteorol. Soc.* **101** S34–S36

Padrón R S, Gudmundsson L, Decharme B, Ducharne A, Lawrence D M, Mao J, Peano D, Krinner G, Kim H and Seneviratne S I 2020 Observed changes in dry-season water availability attributed to human-induced climate change *Nat. Geosci.* **13** 477–81

PERMOS 2021a *Swiss Permafrost Bulletin 2019/2020* ed J Noetzli and C Pellet p 20

PERMOS 2021b Swiss permafrost monitoring network database (PERMOS database) (https://doi.org/10.13093/permos-2021-01)

Ravanel L and Deline P 2010 Climate influence on rockfalls in high-Alpine steep rockwalls: the north side of the Aiguilles de Chamonix (Mont Blanc massif) since the end of the 'Little Ice Age' *Holocene* **21** 357–65

Ribes A, Zwiers F W, Azaïs J-M and Naveau P 2016 A new statistical approach to climate change detection and attribution *Clim. Dyn.* **48** 367–86

Schuur E A G *et al* 2015 Climate change and the permafrost carbon feedback *Nature* **520** 171–9

Schuur E A G, Vogel J G, Crummer K G, Lee H, Sickman J O and Osterkamp T E 2009 The effect of permafrost thaw on old carbon release and net carbon exchange from tundra *Nature* **459** 556–9

Smith S L *et al* 2021 Permafrost [in "State of the Climate in 2020"] *Bull. Am. Meteorol. Soc.* **102** S293–7

Smith S L, O'neill H B, Isaksen K, Noetzli J and Romanovsky V E 2022 The changing thermal state of permafrost *Nat. Rev. Earth Environ.* **3** 10–23

Stott P A, Gillett N P, Hegerl G C, Karoly D J, Stone D A, Zhang X and Zwiers F 2010 Detection and attribution of climate change: a regional perspective *Wiley Interdiscip. Rev. Clim. Change* **1** 192–211

Stuenzi S M, Boike J, Gädeke A, Herzschuh U, Kruse S, Pestryakova L A, Westermann S and Langer M 2021 Sensitivity of ecosystem-protected permafrost under changing boreal forest structures *Environ. Res. Lett.* **16** 084045

Vasiliev A A, Drozdov D S, Gravis A G, Malkova G V, Nyland K E and Streletskiy D A 2020 Permafrost degradation in the Western Russian Arctic *Environ. Res. Lett.* **15** 045001

Zhang X, Zwiers F W, Hegerl G C, Lambert F H, Gillett N P, Solomon S, Stott P A and Nozawa T 2007 Detection of human influence on twentieth-century precipitation trends *Nature* **448** 461–5

Zhao L *et al* 2020 Changing climate and the permafrost environment on the Qinghai–Tibet (Xizang) plateau *Permafr. Periglac. Process.* **31** 396–405

Zwiers F W and Zhang X 2003 Toward regional-scale climate change detection *J. Clim.* **16** 793–7